Bulletin of the Seismological Society of America, Vol. 96, No. 5, pp. 1729–1741, October 2006, doi: 10.1785/0120050200

A Study of the 14 November 2001 Kokoxili Earthquake: History and Geometry of the Rupture from Teleseismic Data and Field Observations

by Audrey Tocheport, Luis Rivera, and Jérôme Van der Woerd

Abstract A study of the 14 November 2001 Kokoxili earthquake is performed to estimate the source parameters from teleseismic body-wave inversion. The earthquake broke the western Kusai Hu segment of the east–west trending Kunlun strike-slip fault, with the presence of surface rupture traces over 400 km. This event of M_w 7.8 (Harvard CMT, 2001) was followed by moderate but continuous seismic activity. We apply an inversion method of complex body waves with multiple subevents (Kikuchi and Kanamori, 1991) to model the waveforms and to understand the rupture process. Field observations are used to constrain the inversion and to evaluate the solution. Considering the western complexities of the Kusai Hu segment, we invert the first part of the data to model the initiation of the rupture. The rupture is found to begin on the fault branch lying southwest of the Buka Daban Peak. Although the rupture propagates dominantly eastward, some subevents systematically appear to the west of the epicenter. Then, an inversion of the complete body-wave traces shows that the rupture propagated unilaterally eastward along the straight part of the Kusai Hu segment.

Introduction

The 14 November 2001 Kokoxili earthquake M_w 7.8 occurred north of the Tibetan plateau, along the Kunlun fault with a rupture length of over 400 km (Lin *et al.*, 2002; Van der Woerd *et al.*, 2002a; Xu *et al.*, 2002) (Fig. 1a). This event is one of the largest continental strike slips recorded in the past century. Despite the large size of this earthquake, it did not cause much damage because it occurred in an almost unpopulated region, the nearest large city, Golmud, lying 150 km away.

The Kunlun fault is a major east–west sinistral strike-slip fault that runs for more than 1600 km from 86° E to 105° E along the eastern Kunlun range, crossing parts of the Xinjiang, Xizang, and Qinghai provinces. During the twentieth century, the seismicity of the Kunlun fault was sparse but continuous with several moderate and large earthquakes associated with the Kunlun fault. The largest earthquakes are the 1937 earthquake of M 7.5 that ruptured most of the Dongxi Co segment (Jia *et al.*, 1988) and the 1997 Manyi earthquake of M_w 7.6 that broke the Manyi segment producing a surface rupture of about 170 km (Peltzer *et al.*, 1999; Van der Woerd *et al.*, 2002a,b) (Fig. 1b).

The 2001 Kokoxili event ruptured mainly the Kusai Hu segment of the Kunlun fault, which is located between the 1937 and 1997 epicenters. Harvard CMT (2001) estimates the magnitude M_w at 7.8 and locates the centroid eastward of the epicenter at 35.80° N 92.91° E on the Kusai Hu segment near the Kusai Lake.

Field investigations show that the coseismic surface rupture extends about 435 km from nearly 90.2° E west of the Buka Daban Peak to 95° E, east of the Kunlun Pass (Lin *et al.*, 2003; Xu *et al.*, 2002). The whole surface rupture has been mapped in the field and shows a 30-km-long ruptured segment to the west and the main 350-km one separated by an extensional step-over graben system of about 40 km long (Klinger *et al.*, 2005b) (Fig. 1b, c). The observed displacements correspond essentially to a pure left-lateral strike-slip motion on subvertical faults. Coseismic displacements were measured by different teams (Lin *et al.*, 2002; Van der Woerd *et al.*, 2002a, 2003; Klinger *et al.*, 2003, 2004, 2005a,b; Fu *et al.*, 2005; Lasserre *et al.*, 2003, 2005; Li *et al.*, 2005; Xu *et al.*, 2006) along the rupture after the 2001 earthquake. First field investigations (Lin *et al.*, 2002) described coseismic rupture with displacements up to 16 m, which, however, were not corroborated by other teams and studies (Xu *et al.*, 2002; Klinger *et al.*, 2005a,b; Lasserre *et al.*, 2005; Xu *et al.*, 2006). The coseismic slip ranges mostly between 3 and 5 m and with maximum about 8–10 m 250 km east of the epicenter (Xu *et al.*, 2002; Klinger *et al.*, 2005a; Lasserre *et al.*, 2005).

The Kokoxili earthquake was recorded by regional and teleseismic networks allowing the study of its source history (Bouchon and Vallée, 2003; Lin *et al.*, 2003; Rivera *et al.*, 2003; Antolik *et al.*, 2004; Ozacar and Beck, 2004). These seismic studies, combined with geologic observations, pro-

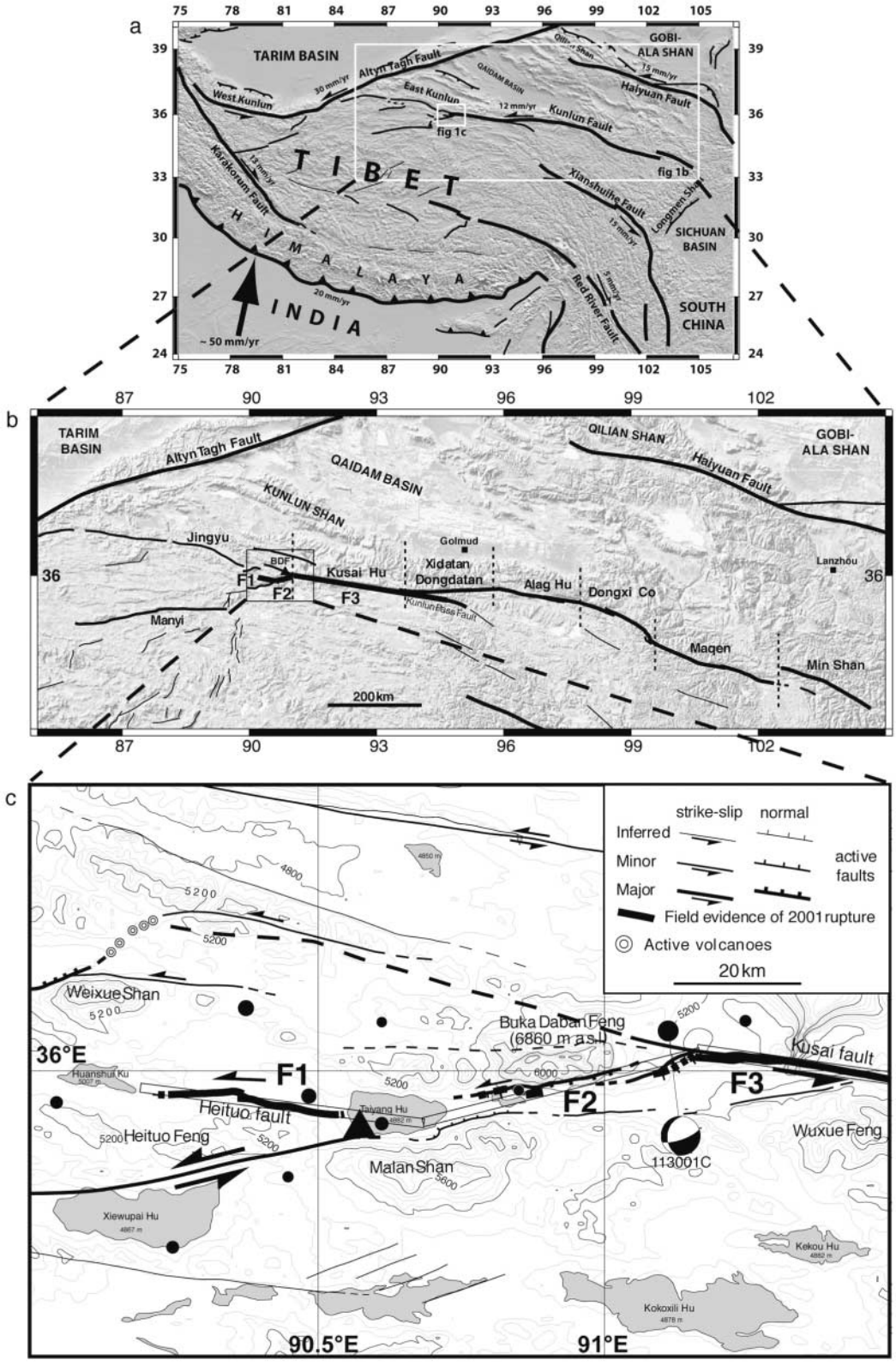

Figure 1. (a) Simplified map of major faults in and around the Tibet Plateau. Faults and kinematics modified from Tapponnier *et al.* (2001b). (b) First-order segmentation of the Kunlun fault modified from Van der Woerd *et al.* (1998). (c) Detailed map of the faults involved in the 2001 Kokoxili earthquake from field evidence. The post-2001 seismicity from the IRIS SeismiQuery events search for events having a $M_b > 4.0$ is mapped. The Harvard focal mechanism of the main aftershock of M_w 5.2 is indicated. The large triangle corresponds to the epicenter relocation of Engdahl (2002). Open rectangles outline simplified faults F1, F2, and F3 used in inversion.

vide a picture of the rupture with an initiation in the west, near the Buka Daban Feng summit, and an eastward propagation with supershear rupture velocity (Bouchon and Vallée, 2003) where large displacements have been observed (Lin *et al.*, 2002; Xu *et al.*, 2002). Most of the rupture is a simple eastward propagation, except in the epicentral area where several fault branches connect and where the rupture mechanisms vary.

Although the overall propagation of the rupture seems to be understood, its initiation is still under discussion. Indeed, slightly different fault geometries of the western Buka Daban Peak region were used to model the rupture, either as an almost uniform segment (Lin *et al.*, 2003) or as two segments with distinct orientations (Fig. 1c) (Antolik *et al.*, 2004; Ozacar and Beck, 2004). The directions of propagation on the different segments are also not well resolved. The lack of detailed fault maps to precisely constrain the complex geometry of this fault branching and the poor sensitivity of teleseismic body waves to such details explain the difficulty in understanding the rupture history in this region.

In this study, we invert teleseismic body waves taking into account our own field observations and those from other studies (Klinger *et al.*, 2005b; Lasserre *et al.*, 2005; Xu *et al.*, 2006) to constrain the source parameters and the history of the 14 November 2001 rupture. We use a multiple-event inversion (Kikuchi and Kanamori, 2003) and modify the algorithm to include multiple faults with complex branching. After performing a simple inversion, considering only the main fault to determine a mean focal mechanism, we focus on the rupture initiation history, which is the most complex part of the rupture. We then compute a final inversion including branches in the epicentral region and the main fault.

Tectonic Setting and Field Observations

The Tibetan plateau and the Himalayan mountains result from the Indo-Asia continental collision (Tapponnier and Molnar, 1977; Tapponnier *et al.*, 2001b) (Fig. 1a). Since about 50 Ma, the northward displacement of India is about 5 cm/yr with about 2 cm/yr absorbed in the Himalayan thrusts (Bilham *et al.*, 1997; Lavé and Avouac, 2000). The remaining convergence is absorbed to the north, in and around the Tibetan plateau and in the Tian Shan (Avouac and Tapponnier, 1993).

Although most of the convergence is absorbed by active shortening along the Tibet plateau margins and northeast of Tibet (Peltzer and Saucier, 1996; Meyer *et al.*, 1998), part of it is accommodated by horizontal block motions along large 1000- to 2000-km-long strike-slip faults, such as the Altyn Tagh, Kunlun, Haiyuan, Karakorum, and Xianshuihe faults (e.g., Van der Woerd *et al.*, 1998, 2002b; Lasserre *et al.*, 2002; Mériaux *et al.*, 2004; Chevalier *et al.*, 2005) (Fig. 1a). The Kunlun fault runs south of the eastern Kunlun mountains between the high Tibetan plateau to the south and northeast Tibet with a lower elevation to the north. The fault extends from 86° E to 105° E for about 1600 km, separating two geologically and tectonically different domains. To the south, the high Tibetan plateau, with an average elevation of 4800 m is dominated mostly by oblique, northeast–southwest- or northwest–southeast-trending strike-slip and north–south-trending normal faults (e.g., Armijo *et al.*, 1989; Taylor *et al.*, 2003), whereas to the north, the margin of Tibet, with an average elevation of 3500 m, is dominated by ~east–west-striking strike-slip and thrust faulting (e.g., Meyer *et al.*, 1998; Tapponnier *et al.*, 2001b) (Fig. 1b).

Geomorphic offsets along the Kunlun fault, whose ages were determined by cosmogenic, radiocarbon, or thermoluminescence dating (Van der Woerd *et al.*, 1998, 2000, 2002b; Li *et al.*, 2005) indicate that the long-term slip rate of the Kunlun fault has been about 10–12 mm/yr for the past 40 ka. Together with the measurements of large coseismic offsets this rate allows the determination of the recurrence time of M 7–8 earthquakes to range between 300 and 800 years along the different segments of the fault (Tapponnier *et al.*, 2001a; Van der Woerd *et al.*, 2002b; Li *et al.*, 2005).

Body-Wave Analysis

Data

We use teleseismic *P* and *S* body waves recorded by the broadband seismological stations of the Incorporated Research Institutions for Seismology (IRIS) and GEOSCOPE-programme (G) networks. According to the geographical distribution and the quality of the data we select 41 vertical records of *P* phases and 15 *SH* phases. Figure 2 shows the distribution of the selected stations, which are all within

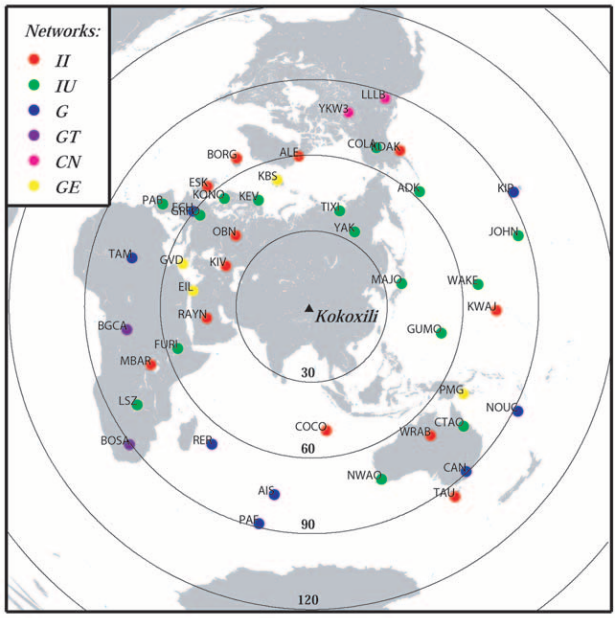

Figure 2. Map of broadband stations used in our inversion distributed at epicentral distances between 30° and 95°.

30° to 95° of epicentral distances to avoid long crustal paths or core mantle boundary (CMB) interactions. We use relative data weighting giving 30–50% of weight to the *SH* phases with respect to 100% to the *P* phases.

African stations are particularly well suited to cover southwestern azimuths with south and east azimuths being covered by island stations in the Indian and Pacific oceans and also in Australia. The north is covered by North American stations. Even if some gaps remain (north of the Indian ocean) the general azimuthal coverage is fairly good.

We converted the broadband high gain seismometer (BH) records into ground displacement, resampled them at 1 sample per second, and performed a horizontal rotation according to the theoretical backazimuth of each station to isolate the *SH* phases.

One important question is the choice of the record length to be used in the waveform inversion. Figure 3 shows the selected vertical records. The first observation is manifest; we are dealing with a very long rupture. Due to the directivity, the apparent duration varies from about 80 sec in the eastern stations (e.g., MAJO, GUMO), to more than 120 sec in the western stations (PAB, TAM). Unfortunately, with the given mechanism and depth, a relatively important *PP* phase comes into the rupture-duration time window. In other words, the *PP* phases originating in the early stage of the rupture interfere with the *P* phases originating in the later stage of the rupture. This effect is especially true in the western, antidirectional, stations. To model the *PP* is not a problem in itself; the problem arises because the *PP* overlaps with the *P* and the resulting interference is strongly dependent on the propagation model. As a result, we would lose the well-known asset of teleseismic modeling of not being very dependent on the global propagation model. We then decided to choose a record length of 130 sec (starting 10 sec before the *P* arrivals). With this choice, we avoid the *PP* interference for most of our stations. The price for that is the loss of the information contained in the latter portion of the western records. An additional potential problem is related to the *PcP* arrival. Fortunately for the mainly strike-slip mechanism we have at hand, the *PcP* amplitudes are very small and they can be neglected without harm.

We systematically observe a weak burst of energy in the first 40 sec followed by a much more energetic one nearly 50 sec after the beginning of the first arrivals. A comparison between the seismograms recorded by eastern and western stations shows that the first bracket of energy seems to be more important in the western stations. On the contrary, the second bracket is much more energetic on the eastern stations. This suggests an eastward propagation of the main rupture along the east–west-trending fault with a complex initiation of the rupture in the west.

Inversion

We use the Kikuchi and Kanamori (1991) teleseismic body-wave inversion program to model these data. The rupture pattern is parameterized as a sequence of subevents distributed on the fault plane determined successively by iterative deconvolution. During the inversion procedure the focal mechanisms of the subevents can be fixed or be determined by the inversion. Mechanism inversion is appropriate to study a complex source process and to understand the mechanism of propagation of the rupture, so we allow the mechanism to vary freely in the inversion.

Each subevent is characterized by a moment tensor, its onset time, and its location on the fault (Kikuchi and Kanamori, 1991). The fault plane is defined by its azimuth, its length, and its dip and is sampled in both dimensions to define a grid on which the subevents are placed during the inversion.

Before performing the inversion itself, it is necessary to calculate the elementary Green's functions for all potential source-station geometries. The propagation in the crust is calculated by using the propagator matrices technique (Haskell, 1953, 1964) in layered media. It concerns the region of the source location but also the structure near the receiver stations. In the Kokoxili earthquake, two models are then necessary for this step; one global for the receivers and another one more adapted to the thick Tibetan crust for the source.

Besides the fault-plane characteristics, other input parameters are needed in this inversion, such as the maximum allowed rupture velocity, the shape of the elementary source time functions (impulse, trapezoid, or triangle), the number of sources, and the duration of the records. The maximum rupture velocity defined here implies a minimum delay between the epicentral time and the rupture time of any given node.

The inversion is nonlinear, and because the problem is not well constrained, it is necessary to impose some additional information to stabilize it. From the preceding discussion, we fixed the source duration to 130 sec. The fault-rupture map is also a rich source of information to fix the initial geometrical parameters. The final normalized residual error measures the quality of the solution and is used to evaluate the fit between the data and the synthetics.

Application to the Kokoxili Earthquake

We made three different inversions to understand the rupture propagation. To know the overall faulting mechanism, we first performed an inversion where the point sources are constrained to lie on the main ruptured fault as seen in the field. Then, to understand the initiation of the rupture more precisely, we modeled the first 35 sec of the records considering the western segments F1 and F2 (Fig. 1b, c) of the Kusai Hu segment. For this second step we had to modify the Kikuchi's algorithm to take into account several fault planes with different trends in a single inversion. The subevents are free to occur on any of the different planes. Finally, we present a complete inversion taking into account the main fault and the western geomet-

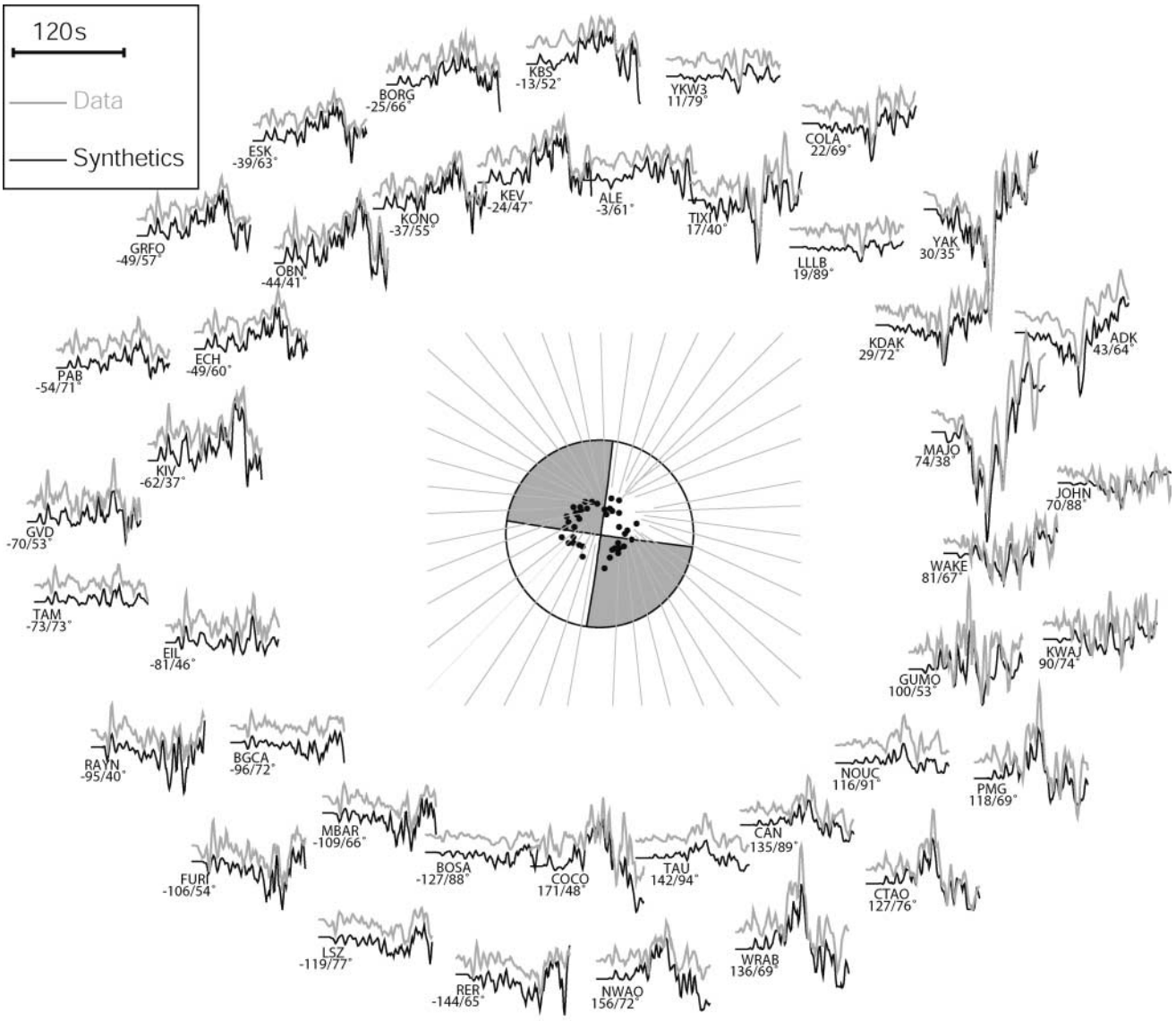

Figure 3. Mean focal mechanism obtained for a multiple-source inversion considering a single fault plane corresponding to the main Kunlun fault (F3 on Fig. 1b) surrounded by the *P* waveforms and the obtained synthetics. The name of the station is indicated for each waveform above the corresponding azimuth and epicentral distance.

rical complexities to model the whole rupture process. In all the inversions, the focal mechanisms are left completely free.

Single Fault Inversion

The overall geometry of the Kusai Hu segment is rather simple without major changes in its orientation. The rupture propagated mainly along the Kusai Hu segment located between 91° E and 94° E. This segment is remarkably straight having an orientation of N90°E in the west, N100°E in the center, and N110°E in the east. Consequently, we modeled the Kusai Hu segment by a unique linear structure having a mean orientation of N100°E, which corresponds to fault F3 (Fig. 1b).

The first inversion is then performed on the fault plane defined previously and on the total duration of the *P* waves. The potential fault grid length is set to 480 km and sampled every 10 km. We also define a maximum depth for the subevents of 20 km with a sampling every 2 km. The source time function is composed by overlapping triangles having half-durations fixed to 3 sec.

The crustal velocity models define the principal boundaries on which reflexions and refractions of waves happen, producing complex waveforms. These models must be chosen carefully to improve the modeling of the waveforms

and reduce the uncertainty of the source parameters. To model the wave propagation in the crust, we use two different models, one for the source and one for the receivers. For the receivers, we use the standard global preliminary reference earth model (PREM) of Dziewonsky and Anderson (1981). For the source, we choose a locally appropriate structure that takes into account the thick Tibetan crust. Different detailed models exist for Tibet. We tested the ASIA model of Kosarev *et al.* (1993) and the CRUST 2.0 model (Laske *et al.*, 2001). All crust models lead to the same modeling results and to a very similar fit between the waveforms and synthetics. The only systematic difference is related to the seismic moment. With PREM, we obtain a moment magnitude of 7.8; with the two others we obtain 7.9. In the following, we use the ASIA model (Kosarev *et al.*, 1993) for the inversions.

The results of the inversion are shown on Figure 3 with the resulting average focal mechanism surrounded by the data and the calculated synthetics. The fit between the data and the synthetics is fairly good overall except for the first weak burst of the *P* waves before 40 sec, which is undermodeled for several stations. The elementary sources tend to cluster where the maximum moment is concentrated near the centroid location. This is observed even if a larger number of elementary sources are allowed in the inversions. The main reason for this behavior of the algorithm is the very high amplitude ratio between the main pulse and the weak first arrival. Indeed, even after some steps of the iterative deconvolution, the misfit around the main pulse remains dominant with respect to the initial amplitudes. This indicates a limitation of the method for the study of complex source time history. To model the entire *P* waveform, we modified the previous inversion and applied a weighting factor to penalize the later segments of the seismograms. This weighting should force the inversion to better explain the first weak part of the records.

The total duration is about 110 sec and the rupture length reaches about 300 km long. The inversion results yield an eastward propagation of the rupture after an initiation in the west. In the next step, we focus on the rupture initiation considering a more realistic geometry to detail the beginning of the propagation.

Rupture Initiation

The 2001 epicenter relocation of Engdahl (2002) (35.894° N, 90.573° E) is located on a secondary strike-slip fault west of the Kusai Hu segment corresponding to branch F1 on Figure 1c. To understand how the rupture propagated from the epicenter to the main Kunlun fault, we model the western fault geometry that comprises the secondary strike-slip fault (F1) and the extensional step-over (F2). This links the first branch (F1) to the main fault F3 (Fig. 1c). We model the two faults F1 and F2 as having a length of 45 km with a sampling of 15 km and use the same definition in depth as for the main plane. In this second step, we invert the first 35 sec of the *P* waves to focus on the very beginning of the propagation.

A test with a single point source preferentially places the source on branch F1 near the epicenter location with a strike-slip mechanism. To improve our model of propagation along these three faults we perform other inversions by progressively adding subevents. For each inversion we carried out sensitivity tests to study the stability of the focal mechanism and the spatiotemporal distribution obtained for each source. This means that for each inversion, we perform about forty other inversions by alternately changing the stations involved and observe the variability of the inverted parameters. The figure in Appendix shows the variations of the spatiotemporal distributions of the sources and of the focal mechanisms for two inversions involving five and eight sources. With five elementary sources or more, the data are well modeled. The *P*-waveform synthetics obtained from the five-sources inversion are shown on Figure 4. The inversion considering the three fault branches improves the fit between waveforms and synthetics by about 10% compared with a unique fault inversion. The synthetics obtained from the unique fault inversion are shown on Figure 5. Eight sources give a good idea of the propagation along the three fault branches. We notice that the last focal mechanisms becomes unstable. Involving more than eight sources in the inversion shows that both focal mechanisms and spatiotemporal distribution of the last sources are not well constrained. With seven and eight sources, we observe that the rupture still begins on the F1 fault with a constant strike-slip mechanism (Fig. 6). Although some sources appear systematically to the west near the initiation point (Figure in Appendix), their associated seismic moment is relatively small. The propagation to the east seems to be a more robust feature. As discussed by Antolik *et al.* (2004) the teleseismic data are not especially well suited to properly constrain the relative location of the subevents. The rupture then passes through the pull-apart (F2) where normal faulting is dominant and finally reaches the main F3 fault at the beginning of the Kusai Hu segment where we recover a strike-slip mechanism.

Multiple Fault Branch Inversion

The third inversion is a combination of the first two described earlier to model the whole rupture process, accounting for the western geometry of the epicenter area. Thus, we invert for multiple subevents, considering the main N100°E striking fault and the two western branches F1 and F2, by inverting the total duration of the body waves of about 120 sec. We apply the same weighting factor as in the first inversion to the beginning of the data and consider the hypocenter relocation of Engdahl (2002) placed at 10 km in depth.

Because the results concerning the elementary sources occurring toward the end of the rupture are sensitive to the number of sources involved in the inversion, we perform a

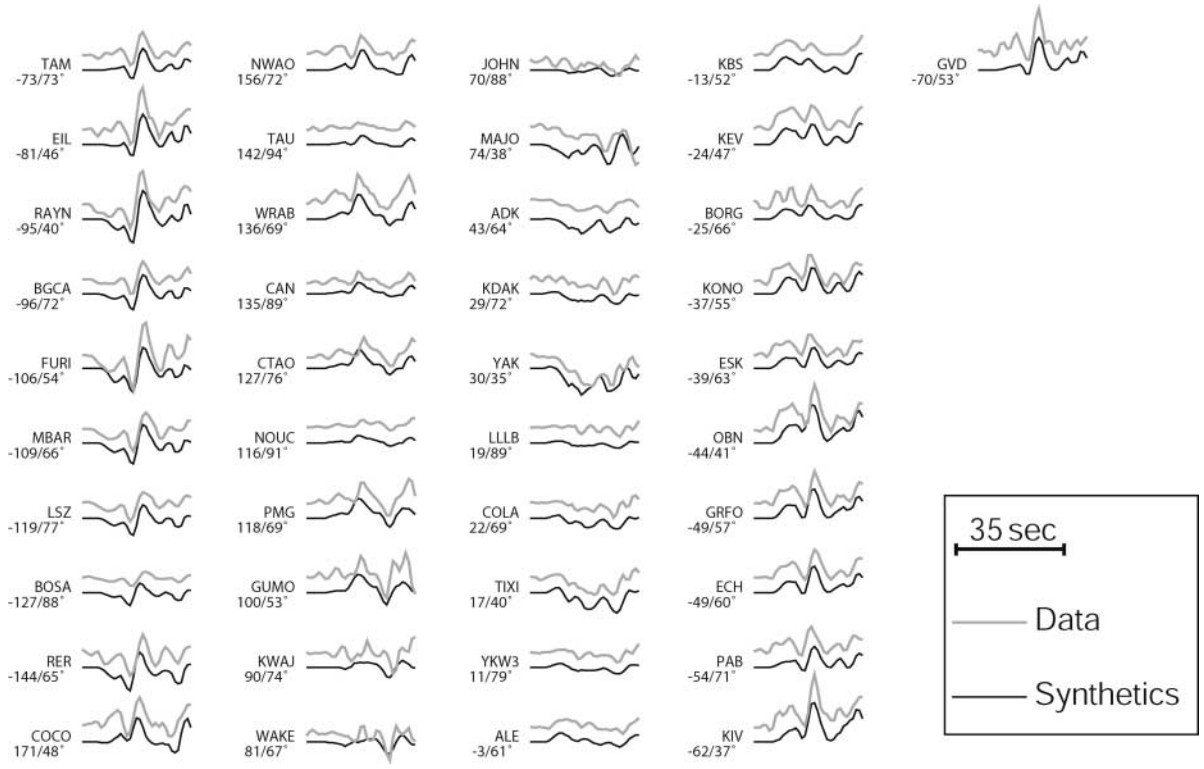

Figure 4. Synthetic seismograms of the *P* waves and the corresponding data resulting from the inversion of the first 35 sec of the data to model the beginning of the rupture considering fault branches F1, F2, and F3 shown on Figure 1c. The name of the station is indicated for each waveform above the corresponding azimuth and epicentral distance.

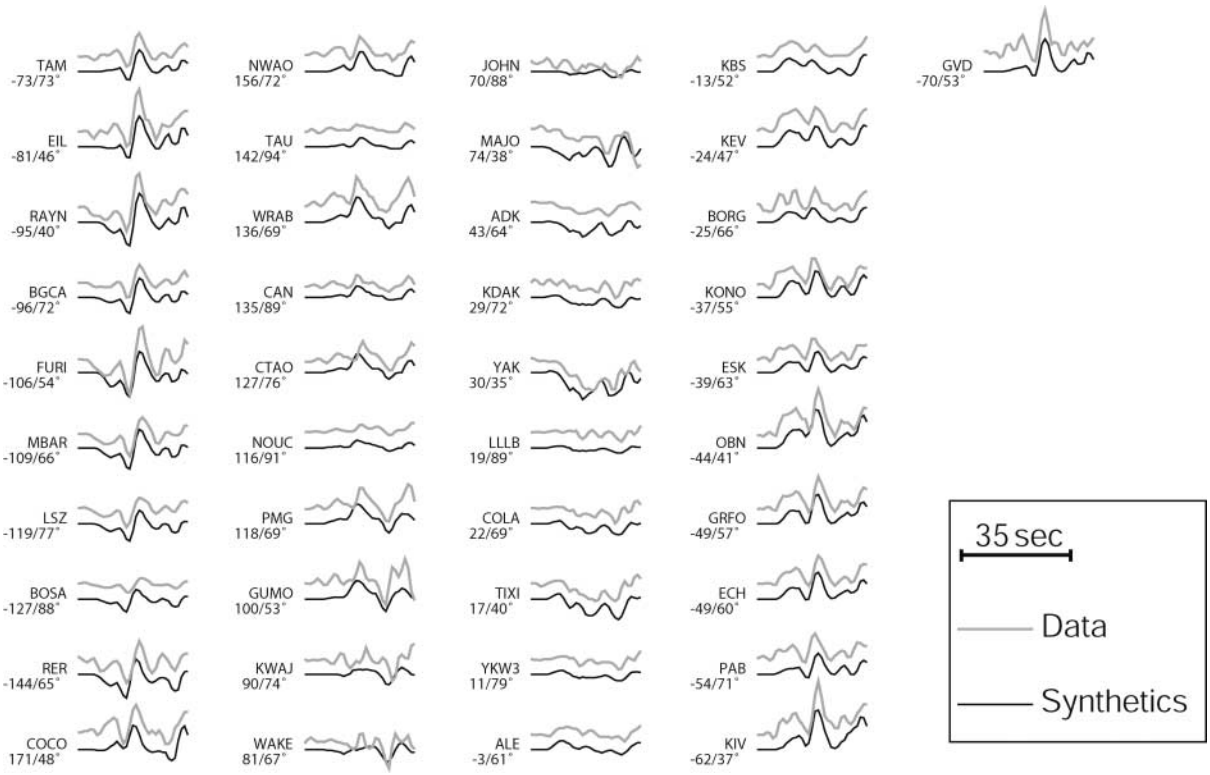

Figure 5. Same as in Figure 4 but considering a unique fault inversion.

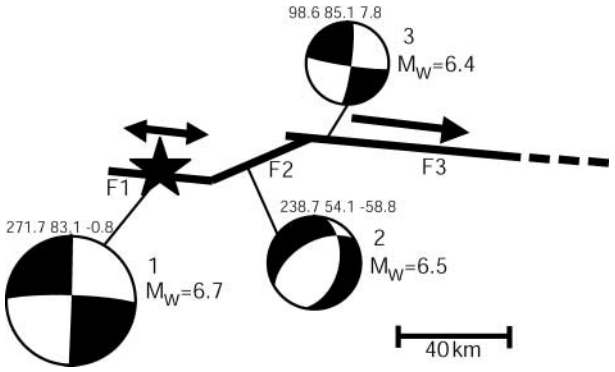

Figure 6. Detail of the Kokoxili rupture initiation process based on the results of the inversion of the first 35 sec. Mean focal mechanisms are shown for each branch, their size being proportional to their seismic moments. Arrows indicate the bilateral or unilateral direction of propagation.

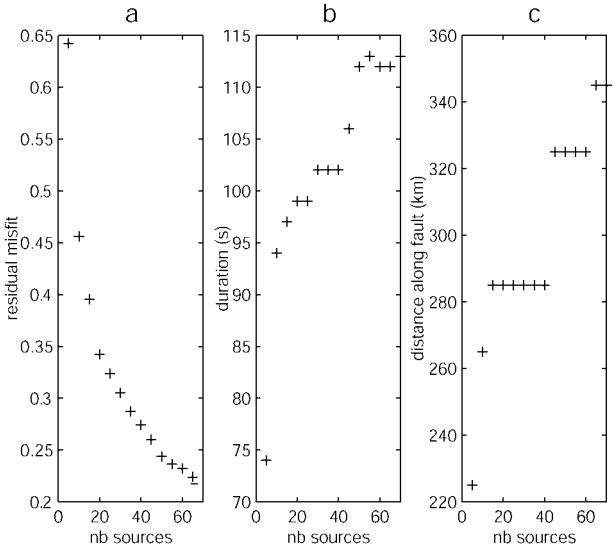

Figure 7. Evolution as a function of the number of sources included in the inversion of (a) the misfit between data and synthetics, (b) the time corresponding to the lastest source, and (c) the distance of the farthest source with respect to the epicenter location.

sequence of inversion tests to see how the obtained parameters vary with the number of sources and to evaluate how many sources are significant. Figure 7 shows the results of the inversions including from 5 to 70 elementary sources. We see that the first 20 elementary sources are necessary to fit the waveforms and that the residual misfit becomes acceptable at about 30 elementary sources (Fig. 7a). Figure 7b, c shows the evolution of the latest and farthest elementary source obtained in the inversions. The duration increases gradually with the number of subevents whereas the evolution of the longest distance increases in steps. The total duration of the signal seems to be explained with about 50 elementary sources and the most eastern source is located at about 350 km from the epicenter.

Figure 8 shows the waveform modeling including 30 elementary sources for some stations compared with the records. The fit is good even for the beginning of the signal, which is improved by the addition of the fault branches F1 and F2. The mean focal mechanism is almost pure strike slip (97.5°, 89.0°, 0.5°) and the obtained total scalar moment released is M_0 9 ∗ 10^{20} N m, which corresponds to a moment magnitude of M_w 7.9. The *SH* waveforms included in this inversion are shown on Figure 9; there is also a good coherence between the data and the synthetics.

The source time function obtained from an inversion considering 30 sources is shown on Figure 10c and reveals two stages. The first stage, corresponding to the first pulse of 40 sec, has a relatively small seismic moment equivalent to 6% of the total, which amounts to a M_w 7.1. The second stage lasts about 80 sec and corresponds to 94% of the total seismic moment, which is equivalent to a M_w 7.9. The average rupture velocity obtained is about 3.4 km/sec, which is lower than the 3.9 km/sec obtained by Bouchon and Vallée (2003) who observed supershear velocity. To understand the rupture propagation we can also look at the position of the most important dislocation points on the different faults shown on Figure 10a,b. The rupture initiates on F1 at the epicenter location at a depth of 10 km and seems to propagate bilaterally during the first 40 sec with a constant and dominant strike-slip mechanism. About 20 sec after the initiation, it passes on F2 through the extentional graben with a strong normal component. It finally reaches the beginning of the Kusai Hu segment (F3) 30 sec after the initiation with a first burst ending at 40 sec at the end of the first stage. Although this burst reaches the Kusai Hu segment, it seems to relate to the first part of the rupture as it belongs to the first 40 sec.

A few seconds after the end of the first stage at about 40 sec, the propagation continues unidirectionally eastward on the main Kunlun fault with a dominant left-lateral strike-slip mechanism corresponding to the second main pulse of the source time function. The focal mechanisms obtained are very stable all along the fault, and the strike of the elementary sources is very similar to the strike of the fault without any constraint imposed on the mechanism. The maximum of the moment rate function happens around 70 sec and is located near the CMT location. One hundred seconds after the beginning of the earthquake, we still observe mostly strike-slip mechanisms and some reverse ones. The focal mechanism is very stable along the fault with a pure left-lateral strike-slip mechanism. The normal component of the subevents observed in the west, near the epicenter location, agrees with the oblique normal strand observed near 91° E (Xu *et al.*, 2006), which may be responsible for the uplift of the Buka Daban Feng (Van der Woerd *et al.*, 2002a). The few thrust subevents found in the east are also consistent with the Kunlun Pass fault being a thrust fault with a strike-slip component (Van der Woerd *et al.*, 2002b).

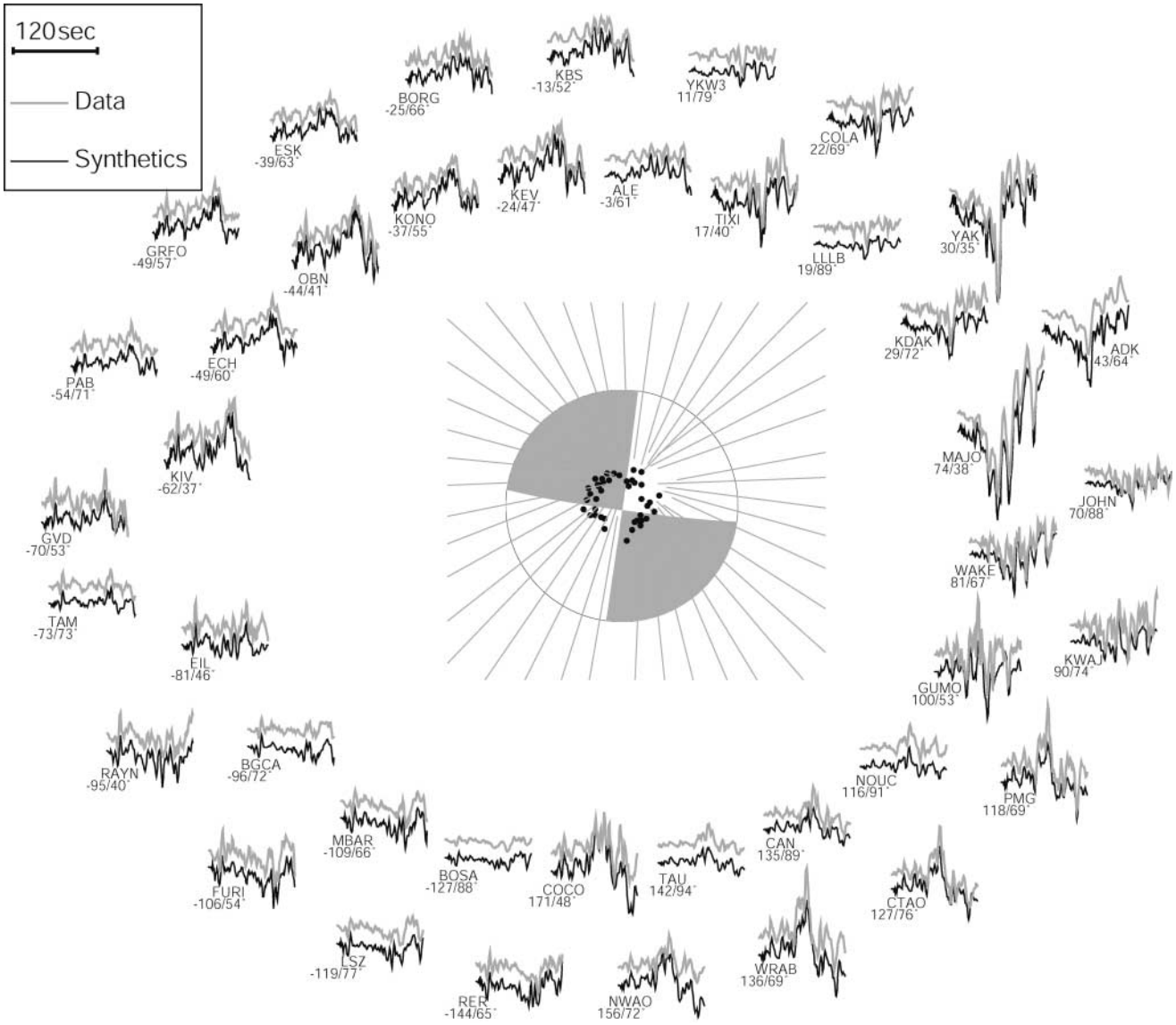

Figure 8. Mean focal mechanism obtained for the complete multiple-source inversion considering the western fault segments F1 and F2 and the main fault F3 (Fig. 1b–c) and 30 sources surrounded by the *P* waveforms and the calculated synthetics. The name of the station is indicated for each waveform above the corresponding azimuth and epicentral distance.

Discussion and Conclusions

Body-Wave Inversion

The teleseismic body-wave inversion results indicate that the 14 November 2001 earthquake had a complex rupture propagation that is best modeled with a multiple events inversion involving three faults. The rupture model shows an initiation on the secondary strike-slip fault F1 with a dominant eastward propagation. It then propagates through the oblique extensional graben F2 before reaching the main Kunlun fault F3 where the rupture continues its way with an eastward unilateral propagation for at least 350 km. Some elementary sources appear about 350 km eastward from the intersection of the main fault and the branch F2, which means that the total length of the rupture is at least 400 km. The mean depth of the sources is 15 km and the mean displacement is about 5 m. We find a dominant strike-slip mechanism for the whole rupture with a normal component in the west at the beginning of the rupture. The distribution of the moment during this earthquake is highly heterogeneous. The first stage represents only about 6% of the total seismic moment while most of the moment concentrates near the location of the CMT (35.8° N, 92.9° E) where the largest coseismic offsets have been measured.

Three different crustal models were tested for the source in the inversion. With the PREM model we find a moment

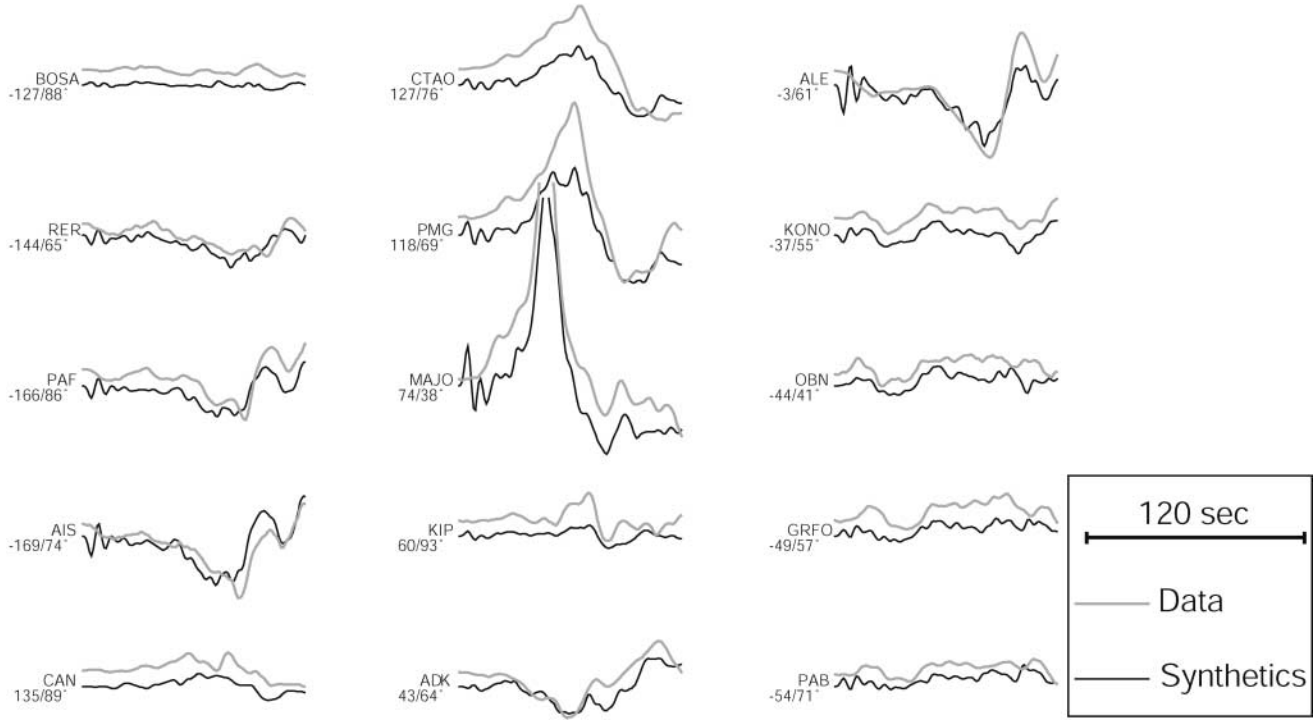

Figure 9. *SH* waveforms and the synthetics obtained for the last complete multiple-source inversion considering faults F1, F2, and F3 (Fig. 1b–c). The name of the station is indicated for each waveform above the corresponding azimuth and epicentral distance.

magnitude of 7.8 compared with the 7.9 obtained using a model more adapted for Tibet, such as ASIA of Kosarev *et al.* (1993) or CRUST 2.0 (Laske *et al.*, 2001). This difference in magnitude can be easily explained directly by the presence of the rigidity μ in the definition of the scalar seismic moment. The use of the potency (Ben-Menahem and Singh, 1981) instead of the seismic moment would avoid this discrepancy because the three models yield similar potency values.

We also tested the influence of the maximum allowed rupture velocity on the results. We observe a constant decrease of the residual misfit function with the increase of the maximum rupture velocity until 3.5 km/sec where the error is minimized. After that point, the rise of velocity increases the misfit function, so 3.5 km/sec seems to be the ideal maximum velocity. However, the error is lowered by only 4% for this velocity in comparison with a maximum velocity fixed to 3.0 km/sec, which is close to the Rayleigh velocity in the brittle crust. Bouchon and Vallée (2003) concluded from a far-regional surface waves study that the rupture started with a sub-Rayleigh rupture velocity of about 2.4 km/sec and then became supershear, reaching 5 km/sec after 100 km of propagation with a mean rupture velocity of 3.9 km/sec. Other teleseismic body-wave studies, such as by Lin *et al.* (2003) or Ozacar and Beck (2004), use a method similar to ours and find a mean rupture velocity of 3.4 km/sec. Similarly, Antolik *et al.* (2004) found a rupture velocity of 3.6 km/sec, which is very similar to our best rupture velocity. However, our inversion does not clearly require supershear rupture velocity to significantly improve the fit to the data. Because teleseismic body waves leave the source with a nearly vertical departure angle, they are less sensitive to the rupture velocity than surface waves.

Comparison with Other Studies

Other seismic body-wave inversions propose different rupture process histories. Lin *et al.* (2003) using a similar inversion method obtain for the strike, dip and rake, respectively (96°, 86°, 7°), close to our average solution and a similar rupture history starting near the epicenter bilaterally before extending unilaterally to the east. The total seismic moment they obtained is $6.5 * 10^{20}$ N m (M_w 7.8) and is lower than the value we propose. They place the epicenter at (36.01° N, 90.10° E), on the western end of the Kusai Hu segment near the interaction with branch F2, which differs from our results. They did not model the western complexities and considered a single east–west fault in the inversion, which limits the interpretation of the beginning of the propagation.

Ozacar and Beck (2004) analyze the source process of the M_w 7.9 Denali earthquake of November 2002 (Eberhart-Phillips *et al.*, 2003) together with the 2001 Kunlun earthquake. They also use the multiple subevents inversion of Kikuchi and Kanamori (1991) to model the two distinct pulses observed on the waveforms. They first invert the ini-

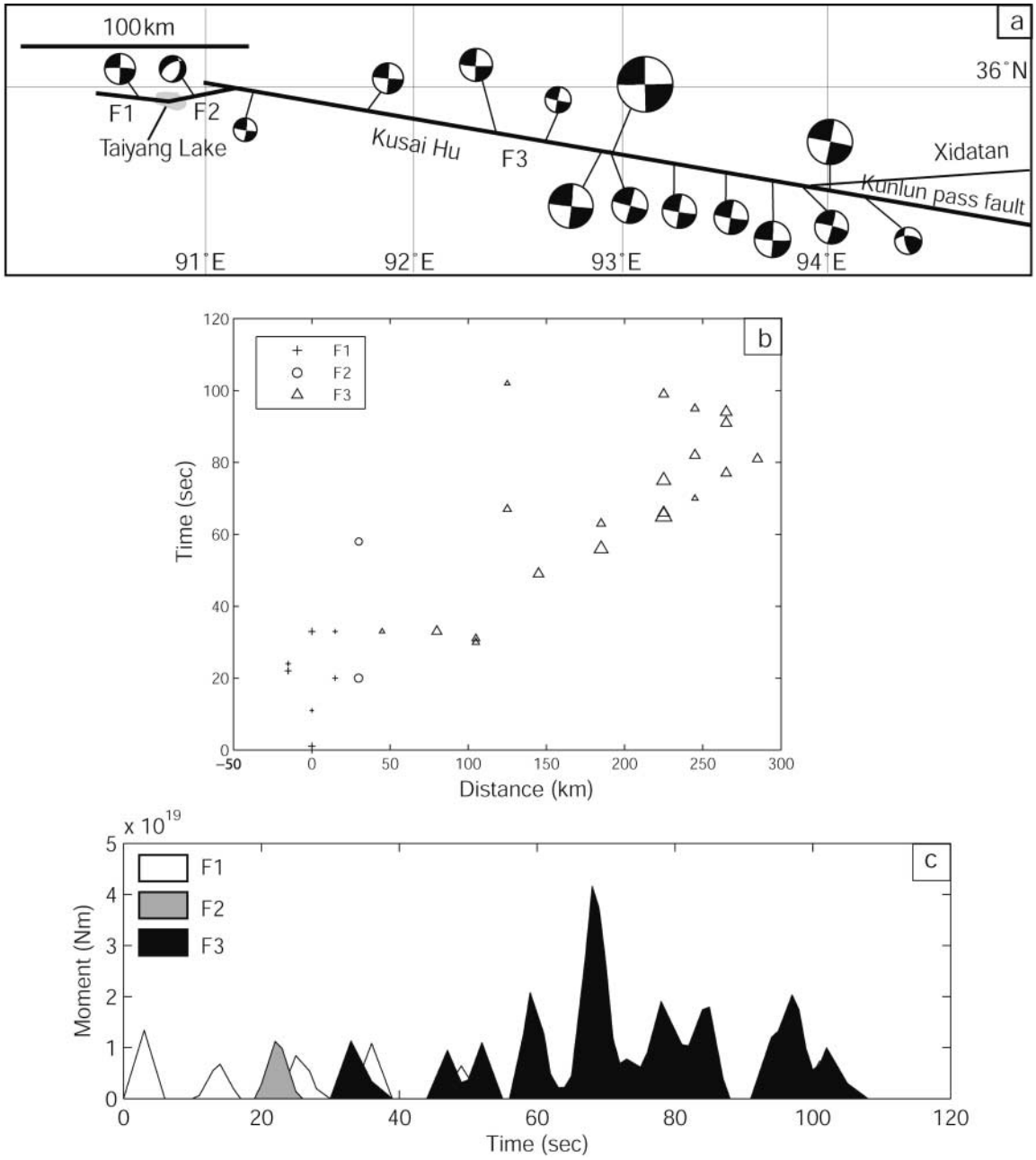

Figure 10. (a) Spatial distribution of the first 15 elementary sources having the most important associated seismic moments along the different fault branches F1, F2, and F3, resulting from the complete inversion involving 30 elementary sources. (b) Spatiotemporal distribution of the 30 elementary sources along the different fault branches F1, F2, and F3. The origin corresponds to the epicenter location. The size of the symbols is relative to the seismic moment of each elementary source. (c) Source time function obtained with 30 elementary sources along the three fault branches F1, F2, and F3.

tial pulse and place the epicenter west of Taiyang Lake (Fig. 1c) and find a very similar rupture history for the first 40 sec. They then invert the residual waveforms and find a unilateral eastward propagation with a left-lateral strike-slip mechanism having the following characteristics (95°, 70°, −15°). Their focal mechanism solution is not very different from ours except for the dip. They found a total seismic moment of $4.55 * 10^{20}$ N m (M_w 7.7) about half of ours.

Antolik *et al.* (2004) used a two-step inversion procedure to recover the rupture process and the slip distribution along the fault. As Ozacar and Beck (2004), they assume propagation on two strike-slip segments linked by an exten-

sional step-over (Antolik *et al.*, 2004). They find rupture propagation starting west of the Taiyang Lake with a strike-slip subevent followed 5 sec later by an oblique-slip subevent having a large normal component remaining in the extentional step-over and a continuous propagation along it before reaching the main segment and propagating unilaterally eastward over 350 km. Our source time function shows that the rupture lasted about 40 sec on the first secondary strike-slip segment, which suggests bilateral propagation on this segment while the rupture already propagated through the step-over about 20 sec after the beginning, before reaching the western part of the main fault at about 30 sec.

All of the three previous studies obtain a source time function, which is mainly concentrated after 40 sec. Our source time function agrees with two-stage propagation. Our first step of propagation in the west lasts 40 sec and involves about 90 km of fault length spread along the three initial branches. Our total seismic moment is $9.0 * 10^{20}$ N m, which is the highest obtained for this earthquake, and the total rupture length is at least 400 km, in agreement with field mapping, which gives a length of 435 km (Xu *et al.*, 2006).

Acknowledgments

The waveforms used in this study were obtained from the IRIS and GEOSCOPE data centers. Most of the figures were produced using Generic Mapping Tools (GMT) software. We thank Michael Antolik, Jeanne Hardebeck, and an anonymous reviewer for their critical and helpful revision of the manuscript.

References

Antolik, M., R. E. Abercrombie, and G. Ekström (2004). The 14 November, 2001 Kokoxili (Kunlunshan), Tibet earthquake: rupture transfer through a large extensional step-over, *Bull. Seism. Soc. Am.* **94,** 1173–1194.

Armijo, R., P. Tapponnier, and T. Han (1989). Late Cenozoic right-lateral strike-slip faulting in southern Tibet, *J. Geophys. Res.* **94,** no. 3, 2787–2838.

Avouac, J. P., and P. Tapponnier (1993). Kinematic model of active deformation in Central Asia, *Geophys. Res. Lett.* **20,** no. 10, 895–898.

Ben-Menahem, A., and S. Singh (1981). *Seismic Waves and Sources*, Springer, Berlin.

Bilham, R., K. Larson, and J. Freymueller, and Project Idylhim members (1997). GPS measurement of present-day convergence across the Nepal Himalaya, *Nature* **386,** 61–64.

Bouchon, M., and M. Vallée (2003). Observation of long super shear rupture during the M_s = 8.1 Kunlunshan (Tibet) earthquake, *Science* **301,** 824–826.

Chevalier, M. L., F. J. Ryerson, P. Tapponnier, R. C. Finkel, J. Van der Woerd, H. Li, and Q. Liu (2005). Slip-rate measurements on the Karakorum Fault may imply secular variations in fault motion, *Science* **307,** 411–414.

Dziewonsky, A. M., and D. L. Anderson (1981). Preliminary reference earth model, *Phys. Earth Planet. Interiors* **25,** 297–356.

Eberhart-Phillips, D., P. J. Haeussler, J. T. Freymueller, A. D. Frankel, C. M. Rubin, P. Craw, N. A. Ratchkovski, G. Anderson, G. A. Carver, A. J. Crone, T. E. Dawson, H. Fletcher, R. Hansen, E. L. Harp, R. A. Harris, D. P. Hill, S. Hreinsdottir, R. W. Jibson, L. M. Jones, R. Kayen, D. K. Keefer, C. F. Larsen, S. C. Moran, S. F. Personius, G. Plafker, B. Sherrod, K. Sieh, N. Sitar, and W. K. Wallace (2003). The 2002 Denali fault earthquake, Alaska: a large magnitude, slip-partitioned event, *Science* **300,** 1113–1118.

Engdahl, E. R. (2002). ftp://ciei.colorado.edu/pub/user/engdahl/ehb (last accessed January 2005).

Fu, B., Y. Awata, J. Du, Y. Ninomiya, and W. He (2005). Complex geometry and segmentation of the surface rupture associated with the 14 November 2001 great Kunlun earthquake, northern Tibet, China, *Tectonophysics* **407,** 43–63.

Harvard Seismology (2001). Centroid Moment Tensor (CMT) catalog search, www.seismology.harvard.edu (last accessed January 2005).

Haskell, N. A. (1953). The dispersion of surface waves on multilayered media, *Bull. Seism. Soc. Am.* **43,** 17–34.

Haskell, N. A. (1964). Radiation pattern of surface waves from point sources in a multi-layered medium, *Bull. Seism. Soc. Am.* **54,** no. 1, 377–393.

Jia, Y., H. Dai, and X. Su (1988). Tuosuo Lake earthquake fault in Qinghai Province, in *Research on Earthquakes Faults in China*, Xinjiang Seismological Bureau, Xinjiang Press, Wurumuqi, 66–71.

Kikuchi, M., and H. Kanamori (1991). Inversion of complex body waves—iii, *Bull. Seism. Soc. Am.* **81,** no. 6, 2335–2350.

Kikuchi, M., and H. Kanamori (2003). Note on Teleseismic Body-Wave Inversion Program, www.eri.u-tokyo.ac.jp/ETAL/KIKUCHI/ (last accessed September 2003).

Klinger, Y., R. Michel, and G. C. P. King (2005a). Evidence for an earthquake barrier model from $M_w \sim 7.8$ Kokoxili (Tibet) earthquake slip-distribution, *Earth Planet. Sci. Lett.* **242,** no. 3–4, 354–364.

Klinger, Y., R. Michel, J. Van der Woerd, X. Xu, and P. Tapponnier (2004). Slip-distribution and rupture pattern of the 14 November 2001, M_w 7.8 Kokoxili Earthquake (China), Presented at AGU Fall meeting.

Klinger, Y., J. Van der Woerd, P. Tapponnier, X. W. Zu, G. King, W. B. Chen, W. T. Ma, G. Peltzer, and D. Bowman (2003). Detailed strip map of the Kokoxili earthquake rupture (M_w 7.8, 14/11/01) from space, Presented at EGS-AGU-EUG Joint Assembly, Nice, France.

Klinger, Y., X. Xu, P. Tapponnier, J. Van der Woerd, C. Lasserre, and G. King (2005b). High-resolution sattellite imagery mapping of the surface rupture and slip distribution of the M_w 7.8, November 14, 2001 Kokoxili earthquake Kunlun Fault, Northern Tibet, China, *Bull. Seism. Soc. Am.* **95,** no. 5, 1970–1987.

Kosarev, G. L., N. V. Peterson, L. P. Vinnik, and S. W. Roecker (1993). Receiver functions for the Tien Shan analog network: Contrasts in the evolution of structures across the Talasso-Fergana fault, *J. Geophys. Res.* **98,** 4437–4448.

Laske, G., G. Masters, and C. Reif (2001). http://mahi.ucsd.edu/Gabi/rem.html (last accessed January 2003).

Lasserre, C., Y. Gaudemer, P. Tapponnier, A. S. Mériaux, J. Van der Woerd, D. Yuan, F. J. Ryerson, R. C. Finkel, and M. W. Caffee (2002). Fast late Pleistocene slip rate on the Leng Long Ling Segment of the Haiyuan Fault, Qinghai, China, *J. Geophys. Res.* **107,** no. B11, 2276, doi 10.1029/2000JB000060.

Lasserre, C., G. Peltzer, Y. Klinger, J. Van der Woerd, and P. Tapponnier (2005). Coseismic deformation of the 2001 M_w = 7.8 Kokoxili earthquake in Tibet, measured by synthetic aperture radar interferometry, *J. Geophys. Res.* **110,** B12408, doi 10.1029/2004JB003500.

Lasserre, C., G. Peltzer, J. Van der Woerd, Y. Klinger, and P. Tapponnier (2003). Coseismic deformation from the M_w 7.8 Kokoxili, Tibet earthquake, from ERS InSAR data, Presented at EGS-AGU-EUG Joint Assembly, Nice, France.

Lavé, J., and J. P Avouac (2000). Active folding of fluvial terraces across the Siwaliks Hills, Himalayas of central Nepal, *J. Geophys. Res.* **105,** no. 5, 735–770.

Li, H., J. Van der Woerd, Y. Klinger, P. Tapponnier, X. Qi, J. Yang, and Y. Zhu (2005). Slip rate on the Kunlun Fault and recurrence time of great earthquake comparable to the 14/11/2001, M_w 7.8 Kokoxili earthquake at Hongshui Gou, *Earth Planet. Sci. Lett.* **237,** 285–299.

Lin, A., B. Fu, J. Guo, Q. Zeng, G. Dang, W. He, and Y. Zhao (2002). Co-

seismic strike-slip and rupture length produced by the 2001 M_s 8.1 central Kunlun earthquake, *Science* **296,** 2015–2017.

Lin, A., M. Kikuchi, and B. Fu (2003). Rupture segmentation and process of the 2001 M_w 7.8 central Kunlun, China, earthquake, *Bull. Seism. Soc. Am.* **93,** 2477–2492.

Mériaux, A. S., F. Ryerson, P. Tapponnier, J. Van der Woerd, R. C. Finkel, X. Xu, Z. Xu, and M. Caffee (2004). Rapid slip along the central Altyn Tagh Fault: morphochronologic evidence from Cherchen He and Sulamu Tagh, *J. Geophys. Res.* **109,** B06401, doi 10.1029/2003JB002558.

Meyer, B., P. Tapponnier, L. Bourjot, F. Métivier, Y. Gaudemer, G. Peltzer, S. Guo, and Z. Chen (1998). Mechanisms of active crustal thickening in Gansu-Qinghai, and oblique, strike-slip controlled, northeastward growth of the Tibet plateau, *Geophys. J. Int.* **135,** 1–47.

Ozacar, A. A., and S. L. Beck (2004). The 2002 Denali fault and 2001 Kunlun fault earthquakes: Complex rupture process of two large strike-slip events, *Bull. Seism. Soc. Am.* **94,** S278–S292.

Peltzer, G., and F. J. Saucier (1996). Present-day kinematics of Asia derived from geologic fault rates, *J. Geophys. Res.* **101,** no. 12, 27,943–27,956.

Peltzer, G., F. Crampé, and G. King (1999). Evidence of nonlinear elasticity of the crust from the M_w 7.6 Manyi (Tibet) earthquake, *Science* **286,** 272.

Rivera, L., J. Van der Woerd, A. Tocheport, Y. Klinger, and C. Lasserre (2003). The Kokoxili, November 14, 2001 earthquake: history and geometry of the rupture from teleseismic data and field observations, Presented at EGS-AGU-EUG Joint Assembly, Nice, France.

Tapponnier, P., and P. Molnar (1977). Active faulting and tectonics in China, *J. Geophys. Res.* **82,** 905–930.

Tapponnier, P., F. J. Ryerson, J. Van der Woerd, A. S. Mériaux, and C. Lasserre (2001a). Long-term slip rates and characteristic slip; keys to active fault behaviour and earthquake hazard, *C. R. Acad. Sci. Ser. II. Sci. Terre Planet.* **333,** no. 9, 483–494.

Tapponnier, P., Z. Xu, F. Roger, B. Meyer, N. Arnaud, G. Wittlinger, and J. Yang (2001b). Oblique stepwise rise and growth of the Tibet plateau, *Science* **294,** 1671–1677.

Taylor, M., A. Yin, F. J. Ryerson, P. Kapp, and L. Ding (2003). Conjugate strike-slip faulting along the Bangong-Nujiang suture zone accommodates coeval east-west extension and north-south shortening in the interior of the Tibetan Plateau, *Tectonics* **22,** no. 4, 1044, doi 10.1029/2002TC001361.

Van der Woerd, J., Y. Klinger, P. Tapponnier, X. Xu, W. Chen, W. Ma, and G. King (2003). Coseismic offsets and style of surface ruptures of the 14 november 2001 M_w 7.8 Kokoxili earthquake (northern Tibet), Presented at EGS-AGU-EUG Joint Assembly, Nice, France.

Van der Woerd, J., A. S. Mériaux, Y. Klinger, F. J. Ryerson, Y. Gaudemer, and P. Tapponnier (2002a). The 14 November 2001, M_w = 7.8 Kokoxili earthquake in Northern Tibet (Qinghai Province, China), *Seism. Res. Lett.* **73,** 125–135.

Van der Woerd, J., F. J. Ryerson, P. Tapponnier, Y. Gaudemer, R. Finkel, A. S. Mériaux, M. Caffee, G. G. Zhao, and Q. He (1998). Holocene left slip-rate determined by cosmogenic surface dating on the Xidatan segment of the Kunlun fault (Qinghai, China), *Geology* **26,** 695–698.

Van der Woerd, J., F. J. Ryerson, P. Tapponnier, A. S. Mériaux, Y. Gaudemer, B. Meyer, R. C. Finkel, M. W. Caffee, G. G. Zhao, and Z. Q. Xu (2000). Uniform slip-rate along the Kunlun fault: Implications for seismic behaviour and large-scale tectonics, *Geophys. Res. Lett.* **27,** 2353–2356.

Van der Woerd, J., P. Tapponnier, F. J. Ryerson, A. S. Mériaux, B. Meyer, Y. Gaudemer, R. C. Finkel, M. W. Caffee, G. G. Zhao, and Z. Q. Xu (2002b). Uniform post-glacial slip-rate along the central 600 km of the Kunlun fault (Tibet), from ^{26}Al, ^{10}Be, ^{14}C dating of riser offsets, and climatic origin of the regional morphology, *Geophys. J. Int.* **148,** 356–388.

Xu, X., W. Chen, W. Ma, G. Yu, and G. Chen (2002). Surface rupture of the 2001 Kunlunshan earthquake (M_s 8.1), northern Tibetan plateau, China, *Seism. Res. Lett.* **73,** 884–892.

Xu, X., W. Ma, G. Yu, P. Tapponnier, Y. Klinger, and J. Van der Woerd (2006). Re-evaluation of surface rupture parameters and faulting segmentation of the 2001 Kunlunshan earthquake (M_w 7.8), Northern Tibetan plateau, China, *J. Geophys. Res.* **111,** B05316, doi 10.102312004JB003488, 2006.

Appendix

Results of the inversion tests of the first 35 sec of the signal including different stations (Figure A1). On the left, spatiotemporal distribution of the sources is shown for all test inversions. On the right, superimposition of all the focal mechanism solutions is shown for all test inversions.

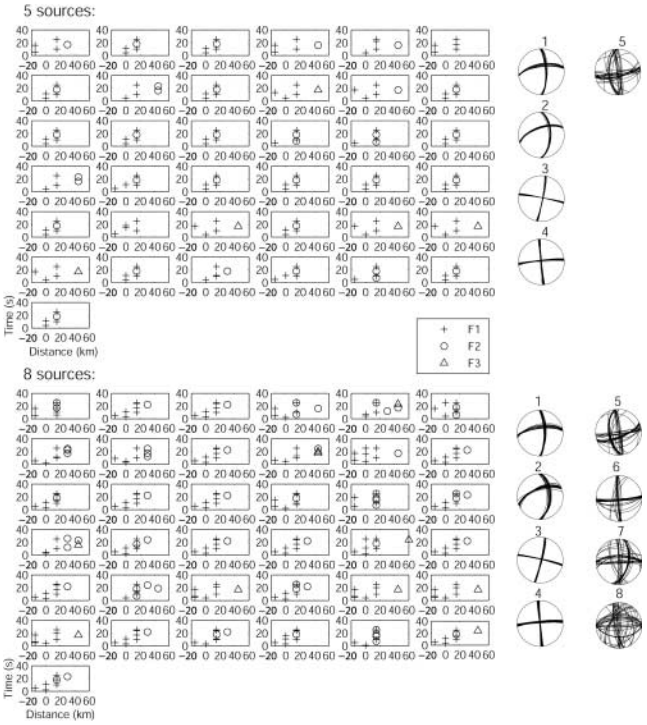

Figure A1.

Institut de Physique du Globe
UMR 7516, 5 rue René Descartes
67084 Strasbourg Cedex, France

Manuscript received 4 October 2005.